

Coherent Terahertz Radiation from a Nonlinear Oscillator of Viscous Electrons

Christian B. Mendl,^{1,2,*} Marco Polini,^{3,4} and Andrew Lucas^{5,6,†}

¹*Technische Universität Dresden, Institute of Scientific Computing,
Zellescher Weg 12-14, 01069 Dresden, Germany*

²*Technische Universität München, Department of Informatics and Institute
for Advanced Study, Boltzmannstraße 3, 85748 Garching, Germany*

³*Istituto Italiano di Tecnologia, Graphene Labs, Via Morego 30, I-16163 Genova, Italy*

⁴*School of Physics & Astronomy, University of Manchester,
Oxford Road, Manchester M13 9PL, United Kingdom*

⁵*Department of Physics, Stanford University, Stanford CA 94305, USA*

⁶*Department of Physics, University of Colorado, Boulder CO 80309, USA*

(Dated: July 22, 2022)

Compressible electron flow through a narrow cavity is theoretically unstable, and the oscillations occurring during the instability have been proposed as a method of generating Terahertz radiation. We numerically demonstrate that the endpoint of this instability is a nonlinear hydrodynamic oscillator, consisting of an alternating shock wave and rarefaction-like relaxation flowing back and forth in the device. This qualitative physics is robust to cavity inhomogeneity and changes in the equation of state of the fluid. We discuss the frequency and amplitude dependence of the emitted radiation on physical parameters (viscosity, momentum relaxation rate, and bias current) beyond linear response theory, providing clear predictions for future experiments.

Introduction.— Generating and detecting Terahertz (THz) radiation (photon frequency in the range ~ 100 GHz–30 THz) are challenging tasks [1]. The reason is that THz radiation lies in the gap between the realms of photonics (on the high-frequency side) and of electronics (on the low-frequency range). Tremendous progress in the generation of THz radiation has been achieved in the last two decades [1]. A number of THz sources have indeed been realized, ranging from THz quantum cascade lasers to LiNbO₃-based optical rectifiers, nonlinear organic crystals, ionized plasmas, difference frequency mixers of optical parametric amplifiers, and accelerators. We refer the reader to Ref. [1] for a recent review.

THz sources that are compact, powerful, tunable, and operating at room temperature are, however, still in great demand for many industrial applications as well as fundamental science, including studying excitations in solids and a plethora of non-equilibrium phenomena. To this end, active research [2, 3] targets the use of two-dimensional (2D) materials, such as graphene, and their van der Waals heterostructures [4, 5]. The main reasons are the small footprint of these materials, the broadband nature and gate tunability of graphene’s optical properties [2], and its exceptionally high electronic quality, unmatched by any other material at room temperature, when encapsulated in atomically flat insulators such as hexagonal Boron Nitride (hBN) [6, 7].

A longstanding proposal for the generation of coherent THz radiation comes from Dyakonov and Shur [8], who noted that a 2D electron system in a hydrodynamic regime exhibits a compressible instability in a cavity with peculiar (but feasible) boundary conditions, which we describe below. In a separate work [9], Dyakonov and Shur proposed also to use hydrodynamic electron fluids to detect THz radiation (for recent work on the topic

see Ref. [10]), which is converted to a dc electrical signal thanks to hydrodynamic nonlinearities.

Despite many experimental attempts, Dyakonov-Shur (DS) *generation* of THz radiation has, to the best of our knowledge, not been reported. On the contrary, down-conversion of THz radiation to a dc signal due to a variety of nonlinearities has been measured [11–17], even as resonantly enhanced by plasmons in high-quality hBN-encapsulated graphene devices [18].

As electrons only behave hydrodynamically in ultra-pure crystals in materials with relatively small Fermi surfaces and strong electron-electron scattering [19–26], one possible obstruction to DS generation of THz radiation has been the challenge of observing the hydrodynamic regime in electron fluids, which has largely been impossible until recent discoveries in graphene [27–32] and GaAs [33–35]: see Ref. [36] for a review.

Given the many experimental efforts to find such instability, and theoretical work suggesting its robustness in the presence of dissipation [8], long-range Coulomb interactions [37], and even in the absence of strong electron-electron interactions [38, 39], we find it quite surprising that the effect has proven so challenging to find. The purpose of this Letter is to answer a simple question: is the instability not observable in experiments because it terminates in an exotic non-equilibrium “state”? Does its endpoint differ in a significant enough way from linear response theory that it would not be detected in existing experimental setups?

We address this question by numerically solving the hydrodynamic equations for electron fluids in the appropriate geometry. Our principal finding is that the endpoint of instability *is a coherent, nonlinear oscillator*, consisting of alternating shock and rarefaction waves bouncing between the ends of the cavity. We analyze the proper-

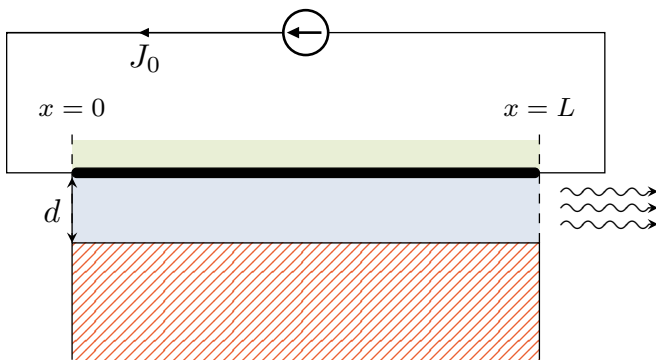


FIG. 1. (Color online) A graphene layer (black) is electrically separated from a metal gate (red hatched); dielectrics such as hBN are usually used to fill the metal-graphene gap providing electrical isolation and also placed above graphene to screen it from impurities. The metal/graphene hybrid forms a capacitor whose charging and uncharging generates power in the THz range. The oscillatory dynamics originates from an instability caused by the presence of bias current in the graphene.

ties of this nonlinear oscillator, including the amplitude and frequency of the emitted radiation, each of which depend on all physical parameters in the problem (viscosity, momentum relaxation rate, etc.). Our results suggest that instability *should be detectable* in present day experiments, and provide further predictions for experiments well beyond the linear stability analysis of Ref. [9].

Setup.—We first describe the basic setup of [8] for generating THz radiation, depicted in Fig. 1. A 2D material, such as graphene, is placed at a distance d from a metallic gate. Dielectric media such as hBN are placed between graphene and the metal gate to provide electrical isolation and above graphene to screen it from contamination. The length of the graphene is L , and the width of the device is w . The graphene/gate act as an effective capacitor. As we will see, the oscillatory dynamics of the electron fluid charges and uncharges this capacitor, and the energy stored in the capacitor can be radiated away through an antenna.

Recent experiments [27–32] demonstrate that the electrons in high quality graphene are well described for temperatures $70 \text{ K} \lesssim T \lesssim 300 \text{ K}$ by a hydrodynamic theory. We denote the electron number density n , thermodynamic pressure $P(n)$, shear viscosity η , momentum relaxation rate γ , and external electric field E . The charge of the electron is $-e$, and its effective mass is m . Assuming equilibrium charge density n_0 and fluid element velocity v_0 , Newton’s Law implies the existence of a steady state with dc current flow through the device, with electron number current

$$J_0 = n_0 v_0 = \frac{-en_0 E}{\gamma m}. \quad (1)$$

In the laboratory, it is not possible to construct a flow with perfectly homogeneous density $n(x, t) = n_0$ and

number current $J(x, t) \equiv n(x, t)v(x, t) = J_0$, where we have introduced the fluid element velocity $v(x, t)$. We model the dynamics of long wavelength perturbations to this steady state using nonlinear hydrodynamics:

$$\partial_t n + \partial_x J = 0, \quad (2a)$$

$$\partial_t J + \partial_x \left(\frac{J^2}{n} + \frac{P(n)}{m} - \frac{\eta}{m} \partial_x \frac{J}{n} \right) = \gamma (n v_0 - J). \quad (2b)$$

The first equation is the continuity equation, while the second one is the Navier-Stokes (momentum balance) equation. The one-dimensional modelling is justified by the translational invariance of the DS boundary conditions introduced below along the direction orthogonal to x [40]. In the main text, we assume the simplified relation

$$P(n) = m v_s^2 n, \quad (3)$$

where v_s is the speed of sound in the fluid and taken to be independent of n . We also define the three relevant dimensionless quantities $\tilde{v}_0 = v_0/v_s$, $\tilde{\eta} = \eta/(m n_0 v_s L) \equiv \nu/(v_s L)$ —where we have introduced the kinematic viscosity $\nu = \eta/(n_0 m)$ —and $\tilde{\gamma} = \gamma L/v_s$. Eqs. (2) and (3) form a minimal model for our hydrodynamic instability. The qualitative conclusions of our study are unchanged by more realistic equations of state $P(n)$, which we derive and discuss in the Supplementary Information (SI).

We study (2) in the spatial domain $0 \leq x \leq L$, subject to the DS boundary conditions

$$n(0) = n_0, \quad (4a)$$

$$J(L) = n_0 v_0, \quad (4b)$$

$$\partial_x J(0) = 0. \quad (4c)$$

The quasinormal modes near equilibrium have frequencies

$$\omega_n = \frac{\pi v_s}{2L} + i \left(\frac{v_0}{L} - \frac{\gamma}{2} - \frac{\pi^2 n^2}{8L^2} \nu \right) + \dots, \quad (5)$$

where \dots denotes terms quadratic in γ , η , and v_0 , and $n = 1, 3, 5, \dots$ is an odd integer. Clearly, whenever $\tilde{v}_0 > \frac{1}{2} \tilde{\gamma} + \frac{\pi^2}{8} \tilde{\eta}$ there is an instability. The main result of this Letter is the numerical determination of the endpoint of this instability.

Endpoint of Instability.—We solved (2) numerically using finite volume methods combined with Strang splitting (see SI for details). We choose parameters v_0 , η , and γ such that $\max(\text{Im}(\omega_n)) > 0$ in order to observe the hydrodynamic instability. The endpoint of this instability is a coherent, nonlinear oscillator, which we numerically observe to be *universal*—neither the amplitude, frequency nor any other features of the nonlinear oscillations depend on the initial conditions: see Fig. 2. This statement remains true even when v_0 is large. In the latter case, Eq. (5) predicts that there are multiple normal modes which are unstable. Fig. 2 shows the dynamics of $n(L, t)$

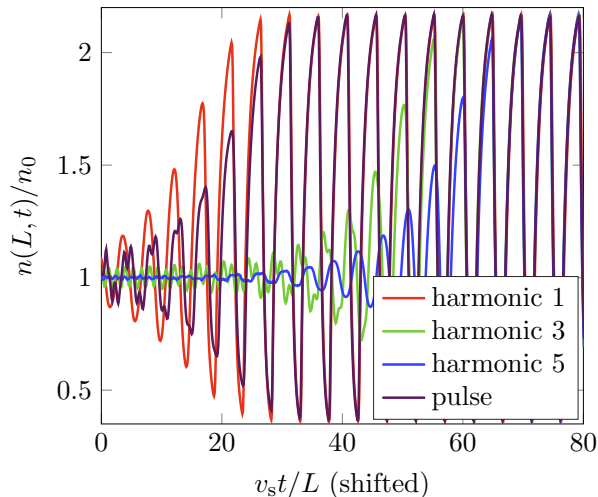


FIG. 2. (Color online) The endpoint of the instability is universal and robust to initial conditions. Parameters are $\tilde{v}_0 = 0.14$, $\tilde{\eta} = 0.01$, and $\tilde{\gamma} = 0.04$; for this choice, (5) predicts that the $n = 3$ mode is just above the instability threshold. t has been offset by a constant for each simulation so that oscillations appear in sync as $t \rightarrow \infty$. With a finite amplitude, sourcing the $n = 5$ harmonic (formally stable) nevertheless ultimately leads to instability.

for multiple different initial conditions at such high v_0 . Generic initial conditions tend towards the same oscillatory attractor solution.

Our simulations demonstrate unambiguously that the endpoint of the instability is a coherent, nonlinear oscillator. Within numerical resolution, there is a period T such that as $t \rightarrow \infty$, $n(x, t) = n(x, t + T)$ and $J(x, t) = J(x, t + T)$. Ten snapshots of the local density and current in the cavity at different points in time are shown in Fig. 3. We interpret these plots as depicting a left-moving shock wave (with wavefront smoothed by viscous effects), and a right-moving “rarefaction wave”. Similar physics is observed for more realistic equations of state, and for models of inhomogeneous cavities (see SI).

THz Radiation.—The remainder of this Letter focuses on the application of this oscillatory attractor to THz radiation generation. In what follows, we propose future experiments in ultra-clean hBN/WSe₂-encapsulated graphene [41] at electron density $n_0 \approx 5 \times 10^{11} \text{ cm}^{-2}$ and room temperature (300 K). In the geometry in Fig. 1, we choose $d = 5 \text{ nm}$, $w = 5 \mu\text{m}$, and $L = 1 \mu\text{m}$. Hydrodynamic effects do persist in this device despite the additional screening of the Coulomb interactions caused by small d . (In fact, it has been experimentally checked that they persist even in extreme devices with d down to $d \sim 1 \text{ nm}$ [42].) In this setup, we estimate (see SI) that $v_s \approx 1.4 \times 10^6 \text{ m/s}$, $\tilde{\eta} \approx 0.03$, and $\tilde{\gamma} \approx 0.11$. The critical bias current beyond which instability occurs is $\tilde{v}_0 \approx 0.09$. Such bias current is accessible in experiment

without undue heating of the phonons [43].

Fig. 4 shows the frequency f of the hydrodynamic oscillator as a function of v_0 and ν , at the endpoint of the instability, defined by $f = 1/T$. At the onset of the instability, $f = v_s/(4L)$ and is set by the oscillation time of a quarter-wavelength fluctuation. In our proposed experiment, $f \approx 375 \text{ GHz}$ lies at the lower end of the THz gap [1]. At higher values of v_0 , we find that the frequency of oscillations always decreases. Our simulations suggest that adding charge (increasing n) to the cavity takes longer at higher v_0 ; the time to remove this extra charge is very slightly decreasing at higher v_0 . We propose that this increased charging time is a consequence of the additional formation time of the shock wave which moves to the left, but do not have an analytic understanding of this effect.

Next, we calculate the maximum power radiated from an antenna in the setup of Fig. 1. Since the charge in the capacitor is $Q(t) = -e \int_0^L dx n(x, t)$, we upper bound the power generated at the fundamental frequency by

$$P \leq \frac{1}{T} \left| \int_t^{t+T} \frac{dt}{T} \frac{Q^2(t)}{2C} \cos\left(\frac{2\pi t}{T}\right) \right|. \quad (6)$$

Here, $C = \epsilon_{zz} \epsilon_0 L w / d$ is the geometrical capacitance of the setup, ϵ_{zz} is the relative out-of-plane permittivity of the dielectric between graphene and the gate, and $\epsilon_0 = 8.854 \times 10^{-12} \text{ F/m}$ the free-space permittivity.

Fig. 5 plots the upper bound (6) on the radiated power for $\epsilon_{zz} \approx 3.3$, i.e. $C \approx 3 \times 10^{-14} \text{ F}$. Clearly, the radiated power vanishes at the onset of the instability, and increases as the bias current further increases. For the experiment suggested above, the scale of radiated power deep in the unstable regime is $\sim 0.1 \text{ mW}$. For more modest bias currents, this level of radiation is reduced, but even extremely close to the onset of instability the radiation can exceed $\sim 0.01 \text{ mW}$. These output powers are easily detectable by using present day THz detectors, such as bolometers [44] or antenna-coupled graphene field-effect transistors [13].

The most serious limitation for observing the instability in experiments is the presence of momentum relaxation. Fig. 6 shows that beyond a critical value of γ , the instability disappears entirely. This can be understood crudely as follows: if $\gamma = \eta = 0$, then $\text{Im}(\omega_n) = \frac{v_s}{2L} \log \left| \frac{v_s + v_0}{v_s - v_0} \right| < 0.45 \frac{v_s}{L}$. Crudely estimating that momentum relaxation decreases $\text{Im}(\omega_n)$ by $\frac{\gamma}{2}$ even when $v_s \sim v_0$, we estimate that $\tilde{\gamma} < 0.9$ is required to see any instability. We numerically determined that $\tilde{\gamma} \lesssim 0.8$ was necessary to observe at least 0.03 mW of radiated power. Keeping in mind that the hBN/WSe₂-encapsulated graphene has a mean free path almost an order of magnitude larger than hBN-encapsulated graphene [6, 7], and that $\tilde{\gamma} \approx 0.1$ even in a relatively short device of $L = 1 \mu\text{m}$, it is quite possible that experiments on hBN-encapsulated graphene thus far could never observe the spontaneous instability.

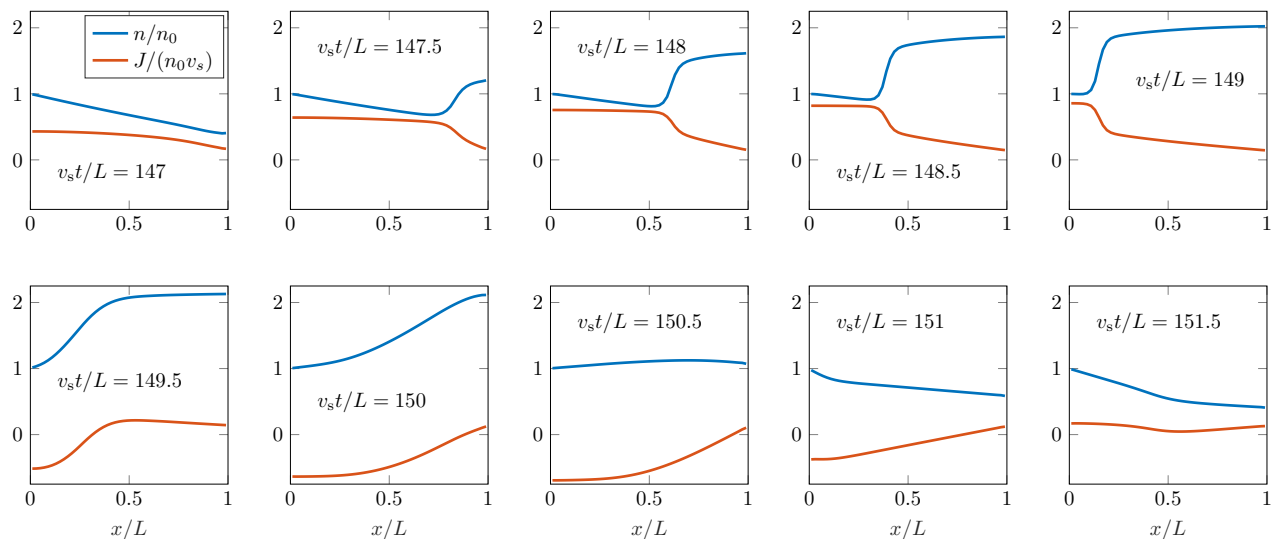


FIG. 3. (Color online) The dynamics of the number density $n(x, t)$ and current $J(x, t)$ throughout a period of the nonlinear hydrodynamic oscillations at the endpoint of the instability. Parameters used are identical to Fig. 2.

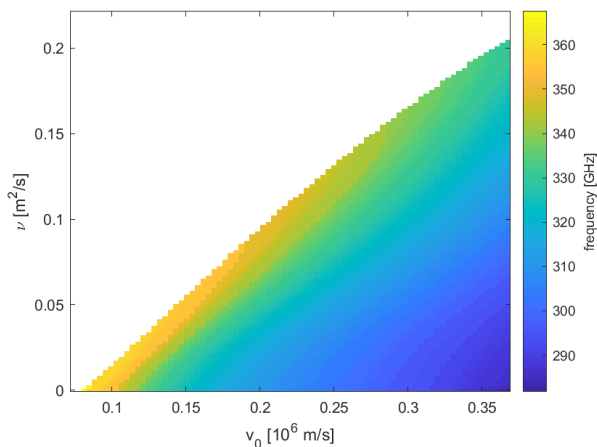


FIG. 4. (Color online) The frequency of the emitted radiation as a function of ν and v_0 ; we have fixed $\gamma = 0.16 \text{ ps}^{-1}$. Parts of parameter space shaded white do not have an instability.

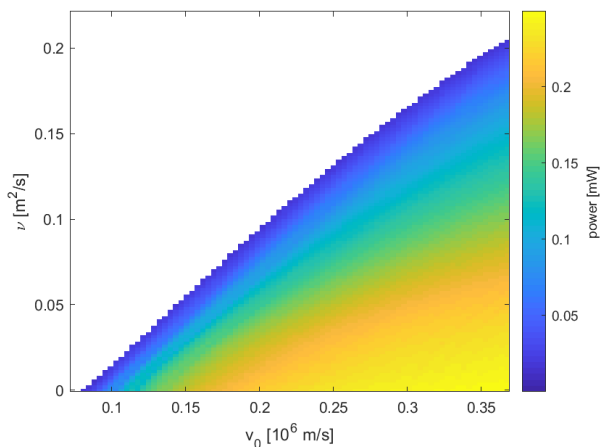


FIG. 5. (Color online) The maximal power dissipated, calculated from Eq. (6), as a function of ν and v_0 . As in Fig. 4, we have fixed $\gamma = 0.16 \text{ ps}^{-1}$. Parts of parameter space shaded white do not have an instability.

A simple idea is to shrink L to be small enough that $\gamma L \ll v_s$. However, unless the electron-electron scattering rate is order(s) of magnitude faster than the electron-impurity scattering rate (which is not quite the case in present day materials), making L very small will push the cavity into a completely ballistic regime: at least within linear response, electron-electron scattering is weak and the dynamics is well described by the kinetic theory of a fluctuating Fermi surface [25]. The instability can persist into this ballistic regime [38, 39], but its modeling requires a nonlinear solution of the Boltzmann equations for a Fermi liquid, beyond the scope of this Letter. The existence of instabilities in this kinetic regime may be very sensitive to boundary conditions [39, 45],

which are difficult to control in experiment. Nevertheless, if the instability can persist deep into the ballistic limit with experimentally realized boundary conditions, then it may be preferable to work in this limit: in hBN/WSe₂-encapsulated graphene, devices generating 1 THz radiation require $L \lesssim 300$ nm, which is not accurately described by hydrodynamics. Tuning the device length from $L=100$ nm to $L=1 \mu\text{m}$ generates radiation across the entire spectrum 0.3-3 THz.

Acknowledgements.— We thank Kin Chung Fong, Christoph Stampfer, and Alessandro Tredicucci for useful discussions. A.L. was supported by the Gordon and Betty Moore Foundation’s EPiQS Initiative

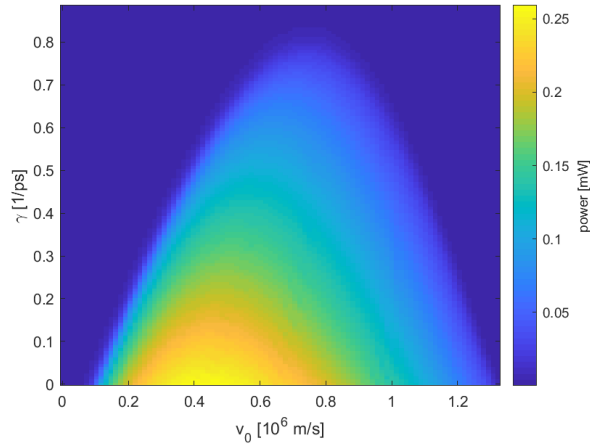


FIG. 6. (Color online) For velocity $|v_0| < v_s$, the instability becomes impossible once momentum relaxation becomes too large.

through Grant GBMF4302. M.P. was supported by the European Union’s Horizon 2020 research and innovation programme under grant agreement No. 785219 - GrapheneCore2.

* christian.mendl@tum.de

† andrew.j.lucas@colorado.edu

- [1] S.S. Dhillon *et al.* “The 2017 terahertz science and technology roadmap”, *J. Phys. D: Appl. Phys.* **50** 043001 (2017).
- [2] F. H. L. Koppens, T. Mueller, Ph. Avouris, A. C. Ferrari, M. S. Vitiello, and M. Polini. “Photodetectors based on graphene, other two-dimensional materials and hybrid systems”, *Nature Nanotechnology* **9**, 780 (2014).
- [3] M. Wang and E.-H. Yang. “THz applications of 2D materials: Graphene and beyond”, *Nano-Structures & Nano-Objects* **15** 107 (2018).
- [4] A. K. Geim and I. V. Grigorieva. “Van der Waals heterostructures”, *Nature* **499** 419 (2013).
- [5] N. Mounet *et al.* “Two-dimensional materials from high-throughput computational exfoliation of experimentally known compounds”, *Nature Nanotechnology* **13** 246 (2018).
- [6] A. S. Mayorov, D. C. Elias, I. S. Mukhin, S. V. Morozov, L. A. Ponomarenko, K. S. Novoselov, A. K. Geim, and R. V. Gorbachev. “How close can one approach the Dirac point in graphene experimentally?”, *Nano Letters* **12** 4629 (2012).
- [7] L. Wang *et al.* “One-dimensional electrical contact to a two-dimensional material”, *Science* **342** 614 (2013).
- [8] M. Dyakonov and M. Shur. “Shallow water analogy for a ballistic field effect transistor: New mechanism of plasma wave generation by dc current”, *Physical Review Letters* **71** 2465 (1993).
- [9] M. Dyakonov and M. Shur. “Detection, mixing and frequency multiplication of terahertz radiation by two-dimensional electronic fluid”, *IEEE Transactions on Electron Devices* **43** 380 (1996).
- [10] D. Svintsov. “Exact solution for driven oscillations in plasmonic field-effect transistors”, *Physical Review Applied* **10** 024037 (2018).
- [11] R. Tauk, F. Teppe, S. Boubanga, D. Coquillat, and W. Knap. “Plasma wave detection of terahertz radiation by silicon field effects transistors: responsivity and noise equivalent power”, *Applied Physics Letters* **89** 253511 (2006).
- [12] M. S. Vitiello, D. Coquillat, L. Viti, D. Ercolani, F. Teppe, A. Pitanti, F. Beltram, L. Sorba, W. Knap, and A. Tredicucci. “Room-temperature terahertz detectors based on semiconductor nanowire field-effect transistors”, *Nano Letters* **12** 96 (2012).
- [13] L. Vicarelli, M. S. Vitiello, D. Coquillat, A. Lombardo, A. C. Ferrari, W. Knap, M. Polini, V. Pellegrini, and A. Tredicucci. “Graphene field-effect transistors as room-temperature terahertz detectors”, *Nature Materials* **11** 865 (2012).
- [14] X. Cai *et al.* “Sensitive room-temperature terahertz detection via the photothermoelectric effect in graphene”, *Nature Nanotechnology* **9** 814 (2014).
- [15] V. Giliberti, A. Di Gaspare, E. Giovine, M. Ortolani, L. Sorba, G. Biasiol, V. V. Popov, D. V. Fateev, and F. Evangelisti. “Downconversion of terahertz radiation due to intrinsic hydrodynamic nonlinearity of a two-dimensional electron plasma”, *Physical Review* **B91** 165313 (2015).
- [16] P. Alonso-González *et al.* “Ultra-confined acoustic THz graphene plasmons revealed by photocurrent nanoscopy”, *Nature Nanotechnology* **12** 31 (2017).
- [17] D. A. Bandurin, I. Gayduchenko, Y. Cao, M. Moskotin, A. Principi, I. V. Grigorieva, G. Goltsman, G. Fedorov, and D. Svintsov. “Dual origin of room temperature sub-terahertz photoresponse in graphene field effect transistors”, *Applied Physics Letters* **112**, 141101 (2018).
- [18] D. A. Bandurin *et al.* “Resonant terahertz detection using graphene plasmons”, *Nature Communications* **9** 5392 (2018).
- [19] R. N. Gurzhi. “Minimum of resistance in impurity-free conductors”, *Journal of Experimental and Theoretical Physics* **17** 521 (1963).
- [20] A. V. Andreev, S. A. Kivelson, and B. Spivak. “Hydrodynamic description of transport in strongly correlated electron systems”, *Physical Review Letters* **106** 256804 (2011).
- [21] A. Tomadin, G. Vignale, and M. Polini. “A Corbino disk viscometer for 2d quantum electron liquids”, *Physical Review Letters* **113** 235901 (2014).
- [22] I. Torre, A. Tomadin, A. K. Geim, and M. Polini. “Non-local transport and the hydrodynamic shear viscosity in graphene”, *Physical Review* **B92** 165433 (2015).
- [23] L. Levitov and G. Falkovich. “Electron viscosity, current vortices and negative nonlocal resistance in graphene”, *Nature Physics* **12** 672(2016).
- [24] A. Lucas, J. Crossno, K. C. Fong, P. Kim, and S. Sachdev. “Transport in inhomogeneous quantum critical fluids and in the Dirac fluid in graphene”, *Physical Review* **B93** 075426 (2016).
- [25] H. Guo, E. Ilseven, G. Falkovich, and L. Levitov. “Higher-than-ballistic conduction of viscous electron flows”, *Proceedings of the National Academy of Sciences (USA)* **114** 3068 (2017).
- [26] T. Scaffidi, N. Nandi, B. Schmidt, A. P. Mackenzie, and

- J. E. Moore. “Hydrodynamic electron flow and Hall viscosity”, *Physical Review Letters* **118** 226601 (2017).
- [27] D. A. Bandurin *et al.* “Negative local resistance due to viscous electron backflow in graphene”, *Science* **351** 1055 (2016).
- [28] J. Crossno *et al.* “Observation of the Dirac fluid and the breakdown of the Wiedemann-Franz law in graphene”, *Science* **351** 1058 (2016).
- [29] R. Krishna Kumar *et al.* “Super-ballistic flow of viscous electron fluid through graphene constrictions”, *Nature Physics* **13** 1182 (2017).
- [30] D. A. Bandurin, A. V. Shytov, L. S. Levitov, R. K. Kumar, A. I. Berdyugin, M. Ben Shalom, I. V. Grigorieva, A. K. Geim, and G. Falkovich. “Fluidity onset in graphene”, *Nature Communications* **9** 4533 (2018).
- [31] M. J. H. Ku *et al.* “Imaging viscous flow of the Dirac fluid in graphene using a quantum spin magnetometer”, [arXiv:1905.10791](https://arxiv.org/abs/1905.10791).
- [32] J. A. Sulpizio *et al.* “Visualizing Poiseuille flow of hydrodynamic electrons”, [arXiv:1905.11662](https://arxiv.org/abs/1905.11662).
- [33] M. J. M. de Jong and L. W. Molenkamp. “Hydrodynamic electron flow in high-mobility wires”, *Physical Review* **B51** 11389 (1995).
- [34] E. V. Levinson, G. M. Gusev, A. D. Levin, E. V. Levinson, and A. K. Bakarov. “Viscous electron flow in mesoscopic two-dimensional electron gas”, *AIP Advances* **8** 025318 (2018).
- [35] B. A. Braem *et al.* “Scanning gate microscopy in a viscous electron fluid”, *Physical Review* **B98** 241304 (2018).
- [36] A. Lucas and K. C. Fong. “Hydrodynamics of electrons in graphene”, *Journal of Physics: Condensed Matter* **30** 053001 (2018).
- [37] M. Dyakonov and M. S. Shur. “Current instability and plasma waves generation in ungated two-dimensional electron layers”, *Applied Physics Letters* **87** 111501 (2005).
- [38] A. P. Dmitriev, V. Yu. Kachorovskii, and M. S. Shur. “Plasma wave instability in gated collisionless two-dimensional electron gas”, *Applied Physics Letters* **79** 922 (2001).
- [39] C. B. Mendl and A. Lucas. “Dyakonov-Shur instability across the ballistic-to-hydrodynamic crossover”, *Applied Physics Letters* **112** 124101 (2018).
- [40] A. Principi, D. Bandurin, H. Rostami, and M. Polini. “Pseudo-Euler equations from nonlinear optics: plasmon-assisted photodetection beyond hydrodynamics”, *Physical Review* **B99** 075410 (2019).
- [41] L. Banszerus *et al.* “Extraordinary high room-temperature carrier mobility in graphene-WSe₂ heterostructures”, [arXiv:1909.09523](https://arxiv.org/abs/1909.09523).
- [42] M. Kim *et al.*, to appear.
- [43] I. Meric, M. Y. Han, A. F. Young, B. Ozyilmaz, P. Kim and K. L. Shepard. “Current saturation in zero-bandgap, top-gated graphene field-effect transistors”, *Nature Nanotechnology* **3** 654 (2008).
- [44] F. Simoens “THz bolometer detectors”, in *Physics and Applications of Terahertz Radiation*, ed. M. Perenzoni and D. J. Paul (Springer, Dordrecht, 2013).
- [45] A. Satou, V. Ryzhii, V. Mitin and N. Vagidov. “Damping of plasma waves in two-dimensional electron systems due to contacts”, *Physica Status Solidi* **B246** 2146 (2009).
- [46] R. J. LeVeque. *Numerical Methods for Conservation Laws* (Birkhauser, 1992).
- [47] R. J. LeVeque. *Finite Volume Methods for Hyperbolic Problems* (Cambridge University Press, 2002).

SUPPLEMENTARY MATERIAL

Numerical Methods

In order to solve the hydrodynamic equations (2) numerically, we use the canonical partitioning into a hydrodynamic conservation law of the form

$$\partial_t u(x, t) + \partial_x f(u(x, t)) = 0 \quad (\text{S1})$$

with $u = (n, J)$ and $f(u) = (J, \frac{J^2}{n} + v_s n)$ (equivalent to the isothermal equations of gas dynamics), the dissipative term $\eta \partial_x^2 \frac{J}{n}$ and the momentum relaxation term $\gamma(nv_0 - J)$. We use finite volume methods [46, 47] on a uniform mesh (width h) for the conservative part and dissipative term, and include momentum relaxation via second order Strang splitting. Thus the numerical flow for a time step τ reads (with \circ denoting composition of functions)

$$\Psi_\tau = \Psi_{\tau/2}^{\text{relax}} \circ \Psi_\tau^{\text{cons}} \circ \Psi_{\tau/2}^{\text{relax}}. \quad (\text{S2})$$

The momentum relaxation step $\Psi_{\tau/2}^{\text{relax}}$ for integrating $\partial_t J = \gamma(nv_0 - J)$ up to $\tau/2$ is simply an exponential decay. The conservative step Ψ_τ^{cons} uses Roe's approximate Riemann solver for isothermal flow combined with a high resolution slope-limiter method [46]. The boundary conditions are treated via ghost cells. Ψ_τ^{cons} also includes the dissipative term, approximated by the second order finite difference quotient $\eta[q(x+h) - 2q(x) + q(x-h)]/h^2$ with $q = \frac{J}{n}$.

The hydrodynamic equations are brought into dimensionless form beforehand; in particular, the one-dimensional spatial domain (length of the cavity) is rescaled from $[0, L]$ to $[0, 1]$. The numerical simulation use a mesh width $h = \frac{1}{50}$. To satisfy the Courant-Friedrichs-Lewy condition [47], a relatively small time step $\tau = 10^{-3}$ is required.

Realistic Pressure for Graphene

In this section we describe simulations of the hydrodynamic equations (2) with the following modified pressure function:

$$P(n) = \frac{1}{2} \frac{n^2 e^2}{C_g} + \frac{\hbar v_F \sqrt{\pi n^3}}{3}, \quad (\text{S3})$$

where the geometric capacitance per unit area is $C_g = \epsilon_{zz} \epsilon_0 / d$. The quantities ϵ_{zz} and ϵ_0 have been defined in the main text after Eq. (6). Eq. (S3) yields a density-dependent sound velocity given by

$$v_s(n) = \frac{v_F}{\sqrt{2}} \sqrt{1 + 8k_F d \alpha_{ee}}, \quad (\text{S4})$$

where $k_F = \sqrt{\pi n}$ is the Fermi wave number and $\alpha_{ee} \equiv e^2 / (4\pi \epsilon_{zz} \epsilon_0 \hbar v_F)$. Eq. (S3) can be understood as follows. The first term corresponds to the energy density stored in the electric fields inside the capacitor—essentially a classical effect due to the geometry. The second term corresponds to the quantum pressure of the electron liquid arising from the Pauli exclusion principle and a Dirac dispersion relation with Fermi velocity v_F , as in monolayer graphene.

Fig. S1 shows both the frequency of the radiation for this more realistic equation of state, together with the amount of power that can be radiated using the setup described in the main text. We emphasize that the qualitative features of these plots are not easily distinguishable from those presented using the minimal model in the main text. As such, we expect that our key qualitative predictions – in particular, the decrease of the frequency of radiation with increasing bias current – are generic and do not depend on microscopic details.

It would be interesting in future work to add two more realistic complications beyond our minimal model (2)—plasmonic effects (long-range Coulomb interactions), together with corrections to the equations of state relating charge, momentum (and energy) currents in monolayer graphene [36].

Inhomogeneity

Lastly, we have checked that the qualitative nature of having a robust oscillator at the endpoint of the instability, with a well defined frequency, is not destroyed by inhomogeneity in the coefficients of the hydrodynamic equations (2): see Fig. S2.

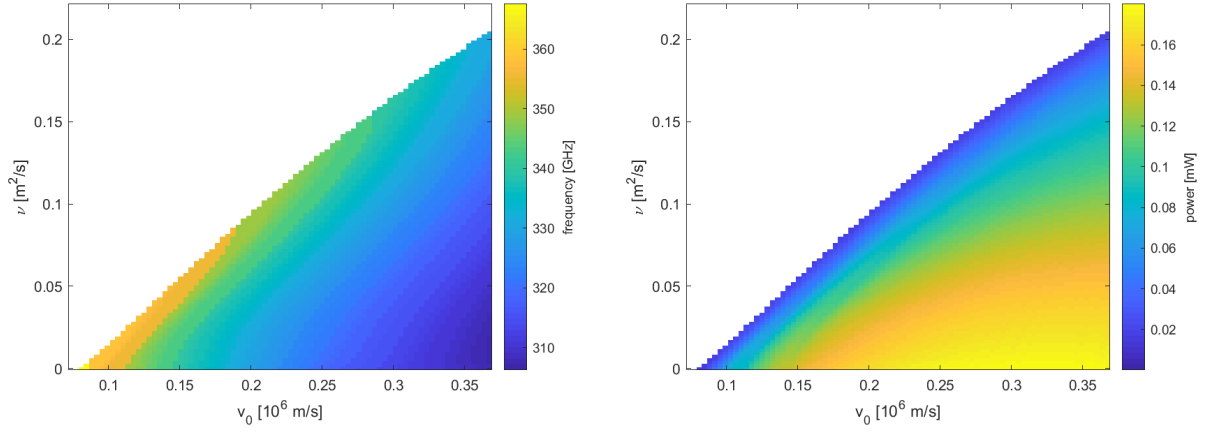


FIG. S1. (Color online) Left: the frequency of the oscillator as a function of ν and v_0 , for the more realistic pressure $P(n)$. Right: the maximal power radiated during the instability.

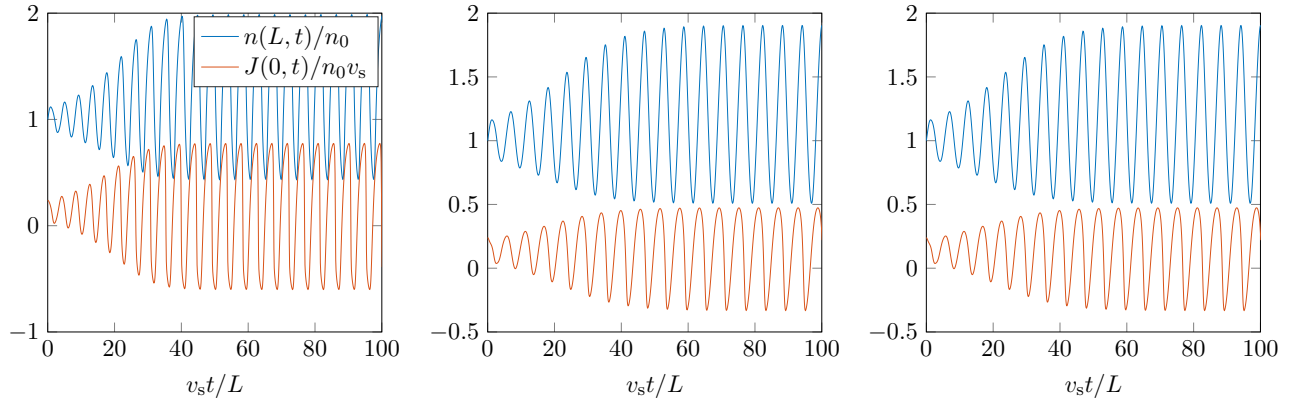


FIG. S2. Simulations of (2) with dimensionless parameters $\tilde{\eta} = 0.03$, $\tilde{\gamma} = 0.04$, $\tilde{v}_0 = 0.14$, with the following modifications to introduce inhomogeneity. Left: $\gamma \rightarrow \gamma \times [1 + 0.8 \cos(2\pi x/L)]$. Middle: $v_s^2 \rightarrow v_s^2 \times [1 + 0.8 \cos(2\pi x/L)]$. Right: $v_s^2 \rightarrow v_s^2 \times [1 + 0.2 \cos(2\pi x/L) + 0.06 \cos(4\pi x/L) - 0.3 \cos(6\pi x/L) + 0.1 \cos(8\pi x/L)]$.